Journal of Alloys and Compounds 489 (2010) 586–591

Contents lists available at ScienceDirect

Journal of Alloys and Compounds

journal homepage: www.elsevier.com/locate/jallcom

Microwave-assisted solid-state decomposition of $La[Co(CN)_6]\cdot 5H_2O$ precursor: A simple and fast route for the synthesis of single-phase perovskite-type $LaCoO_3$ nanoparticles

Saeid Farhadi*, Shahnaz Sepahvand

Department of Chemistry, Lorestan University, Khoramabad 68135-465, Iran

ARTICLE INFO

Article history:
Received 9 August 2009
Received in revised form
19 September 2009
Accepted 22 September 2009
Available online 25 September 2009

Keywords:
Nanoparticles
$LaCoO_3$
Chemical synthesis
Perovskite-type oxide
Inorganic materials
Microwave irradiation

ABSTRACT

Pure and single-phase nanoparticles of perovskite-type $LaCoO_3$ were prepared via microwave-assisted solid-state decomposition of $La[Co(CN)_6]\cdot 5H_2O$ precursor in the presence of CuO powder as a strong microwave absorber within a very short reaction time of 10 min. Product was characterized by X-ray diffraction (XRD), Fourier-transformed infrared spectroscopy (FT-IR), Raman spectroscopy, UV–visible spectroscopy, X-ray photoelectron spectroscopy (XPS), scanning electron microscopy (SEM) and transmission electron microscopy (TEM) and surface area measurement. The method is simple, fast and energy efficient and resulted in fine particles (10–30 nm) with high specific surface area and narrow size distribution. This hybrid microwave heating route is promising for the synthesis of other mixed oxide and related compounds.

1. Introduction

Perovskite-type oxides (ABO_3; A = a rare earth cation and B = a transition metal cation) constitute an important class of strategic materials due to their outstanding properties [1]. The electrical, mechanical, optical, magnetic and catalytic properties these materials find numerous technological uses. These oxides have been used in: solid oxide fuel cells as electrode materials [2–6], chemical sensors [7–10], oxygen-permeating membranes [11] thermoelectric devices [12] and as catalyst for combustion of CO, hydrocarbons and NO_x decomposition [13–19]. For these applications, it is important to prepare high-quality and homogeneous powders with controlled stoichiometry and microstructure. In most cases, the presence of secondary phases will decline in the functional properties, so that single-phase materials are preferred.

Among perovskite-type oxides, $LaCoO_3$ and related materials exhibit interesting electrical and electrocatalytic properties. Also, $LaCoO_3$ has very high electronic conductivity and good ionic conductivity. The properties of this material are strongly dependent on the preparation method which affects its numerous applications.

Generally, $LaCoO_3$ has been prepared by conventional solid-state reaction of pure oxides of La_2O_3 and CoO, carbonates and/or oxalates of metal components at temperature greater than 1000 °C [20–22]. Although the solid-state reaction is very simple, this process is not entirely satisfactory because of several serious drawbacks such as high reaction temperature, long calcination times, introducing impurities during extensive grinding and milling, limited degree of chemical homogeneity, large particle sizes, high aggregation of particles with low specific surface areas and ease of formation of the secondary phases.

In order to overcome above problems, extensive investigations have been performed for preparing finer and more homogeneous $LaCoO_3$ at lower temperatures using soft chemical processes. Various low temperature chemical routes such as coprecipitation [23], decomposition of heteronuclear complex [24–27], mechanochemical synthesis [19], combustion method [28], sol–gel [29] and pechini-type polymerizable complex [30–33] have been reported for obtaining pure phase $LaCoO_3$ nanopowder with high surface area and well-defined chemical compositions. However, most of these processes are either complex or expensive and limit their large-scale production. Therefore, introduction of an inexpensive, green and novel method for preparing pure phase and nano-sized $LaCoO_3$ is still an interesting research topic.

In recent years, the microwave-assisted method has been used extensively for the synthesis of inorganic material [34,35]. This method has unique effects and significant merits such as easy workup, rapid volumetric heating, high reaction rate, short reaction time, energy saving and production of inorganic nanoparticles with

* Corresponding author. Tel.: +98 661 2202782; fax: +98 661 6200098.
E-mail address: sfarhad2001@yahoo.com (S. Farhadi).

0925-8388/$ – see front matter © 2009 Elsevier B.V. All rights reserved.
doi:10.1016/j.jallcom.2009.09.117

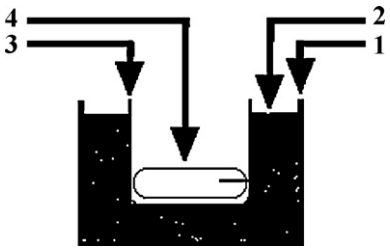

Fig. 1. Schematic illustration of the crucible system: (1) large crucible, (2) CuO powder, (3) small crucible, and (4) precursor pellet.

narrow size distribution as compared with other methods. Various inorganic nanomaterials have been synthesized using microwave irradiation technique for different applications [36–44]. In this context, we have prepared perovskite-type $LaFeO_3$ nanoparticles from $La[Fe(CN)_6]\cdot 5H_2O$ precursor under microwave irradiation with assistance of SiC as a strong microwave absorber [45].

In this work, we report a fast, simple and clean route to prepare $LaCoO_3$ nanoparticles in pure phase through microwave-assisted solid-state decomposition of $La[Co(CN)_6]\cdot 5H_2O$ precursor in the presence of CuO as a secondary heater to initiate the reaction. The obtained product was identified by X-ray diffraction (XRD), Fourier-transformed infrared spectroscopy (FT-IR), Raman spectroscopy, UV–visible spectroscopy, X-ray photoelectron spectroscopy (XPS), scanning electron microscopy (SEM) and transmission electron microscopy (TEM). In addition, the possibility for synthesizing other Lanthanide cobaltites, $LnCoO_3$ (Ln = Sm, Nd, Gd), has been discussed.

2. Experimental

2.1. Preparation

First, the $La[Co(CN)_6]\cdot 5H_2O$ precursor was prepared by mixing aqueous solutions of equal molar of $K_3[Co(CN)_6]$ and $La(NO_3)_3\cdot 6H_2O$ with continuous stirring [45]. The mixture was stirred at room temperature for 30 min. The resulting yellowish precipitate was separated and washed with water, ethanol, and diethyl ether and dried in air. To prepare $LaCoO_3$ nanoparticles, the precursor powder was pressed into pellets (10 mm × 3 mm) with a pressure of 200 MPa and put in a porcelain crucible. This crucible was placed in the middle of another larger porcelain crucible filled with CuO powder as a secondary microwave absorber. A schematic diagram of the crucible system is shown in Fig. 1. This assembly was placed in a domestic microwave oven (LG-30L, 900 W, MW frequency 2.45 GHz) and irradiated at the highest power level of 900 W in air. After an irradiation time of 10 min that the CuO powder became fully red hot, the complete decomposition of the precursor pellet was occurred. The product was cooled to room temperature and collected for the characterization. In a similar manner above, other lanthanide cobaltites were prepared from the decomposition of their corresponding $Ln[Co(CN)_6]\cdot 5H_2O$ precursors.

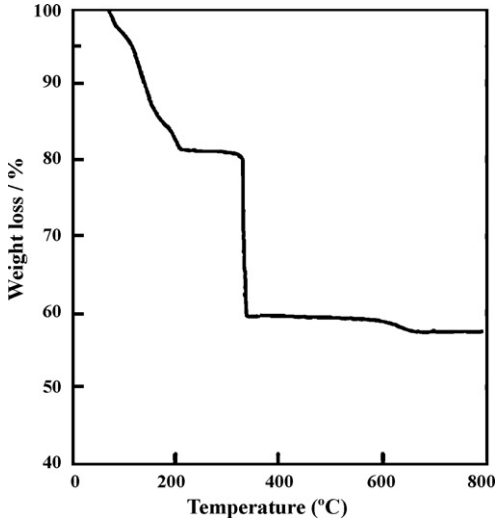

Fig. 2. TG curve of $La[Co(CN)_6]\cdot 5H_2O$.

2.2. Characterization

The crystal structure and phase compositions of the obtained product were identified with a Bruker D8 Advance X-ray diffractometer using Cu Kα radiation (λ = 0.15418 nm). Infrared spectra were recorded on a Schimadzu system FT-IR 8400 spectrophotometer using KBr pellets. Thermogravimetric analysis of the precursor was performed in air using a STA 449C thermal analyzer. Raman spectrum measurement was carried out on a Spex 1403 Raman spectrometer. Optical absorption spectrum was recorded on a Shimadzu UV–vis spectrophotometer with the wavelength rang of 200–500 nm at room temperature. The sample for UV–vis studies was well dispersed in distilled water to form a homogeneous suspension by sonicating for 25 min. The morphology and particle sizes of product were revealed by a transmission electron microscope (TEM, LEO-906E) and a scanning electron microscope (SEM, Philips XL-30). The TEM image of product was obtained at the accelerating voltage of 200 kV. TEM sample was prepared by dropping the ethanol dispersion on a carbon-coated copper grid. Specific surface area was calculated by the BET method using nitrogen. XPS measurement was performed on a PHI-5300/ESCA system with Mg Kα radiation as the exciting source.

3. Results and discussion

3.1. Characterization of $LaCoO_3$ nanoparticles

In the present study, $LaCoO_3$ nanoparticles were prepared from the decomposition of $La[Co(CN)_6]\cdot 5H_2O$ precursor under microwave irradiation in the presence of CuO powder. It is known fact that in microwave synthesis of materials at least one of the reactants should be a good microwave absorber. When the reactants are poor absorbers, hybrid method in the presence of a strong absorber is a suitable route. In the present study, the $La[Co(CN)_6]\cdot 5H_2O$ precursor does not absorb microwaves and remained unchanged without the assistance of a strong secondary absorber. For this purpose, CuO powder was used as shown in Fig. 1. At the initial stage, the microwave radiation is mainly absorbed by the CuO powder and its temperature increases very quickly. Subsequently, the sample is heated by the hot heating medium of CuO and the $LaCoO_3$ can be obtained within several minutes. It seems that the decomposition of $La[Co(CN)_6]\cdot 5H_2O$ pellet was accompanied by the evolution of various gases (such as CO_2, NO_x and water vapor) and this gas evolution breakdown the pellet to a fine powder. The microwave reaction involved in the formation of $LaCoO_3$ is as follows:

$$La[Co(CN)_6]\cdot 5H_2O \xrightarrow[\text{Solid-state reaction in air}]{\text{microwave+CuO}} LaCoCO_3 + 6CO_2 + 6NO_x + 5H_2O$$

Thermal behavior of the $La[Co(CN)_6]\cdot 5H_2O$ precursor was first investigated with thermal gravimetric analysis (Fig. 2). From TG curve in Fig. 2, two major weight losses were observed. The first weight loss is attributed to the loss of five molecules of crystallization water, whereas second one is due to the decomposition of the cyanide groups, followed by a gradual weight loss until 650 °C. The total weight loss is about 42%, which is close to the theoretical value for the formation of $LaCoO_3$ according with the above chemical equation.

Fig. 3 shows the XRD pattern of $La[Co(CN)_6]\cdot 5H_2O$ precursor. All diffraction data, especially interplanar *d*-spacing assigned to the peaks in this pattern match very well with those reported in literature for the pure $La[Co(CN)_6]\cdot 5H_2O$ (JCPDS card no. 36-0674).

Fig. 4 shows the XRD pattern of the obtained powder from the decomposition of $La[Co(CN)_6]\cdot 5H_2O$ precursor under microwave irradiation. From the comparison of Fig. 4 with Fig. 3, it is very clearly evident that all diffraction peaks related to $La[Co(CN)_6]\cdot 5H_2O$ were disappeared and the new peaks were appeared. All diffraction peaks in Fig 4 can be readily indexed to rhombohedral structure of perovskite-type $LaCoO_3$ with lattice

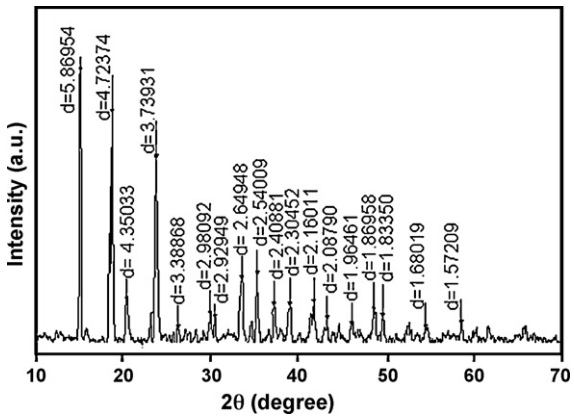

Fig. 3. XRD pattern of the $La[Co(CN)_6]\cdot 5H_2O$ precursor.

constants $a_0 = b_0 = 0.5441$ and $c_0 = 1.3088$ nm (JCPDS, card no.: 25-1060). The splitting of peak at $2\theta = 33.5$ confirms rhombohedral symmetry of $LaCoO_3$. The diffraction angle, interplanar d-spacing and intensity of the characteristic peaks of the product are well consistent with those of the standard JCPDS card of $LaCoO_3$. No characteristic XRD peaks of possible impurity phases such as $La(OH)_3$, La_2O_3, La_2CO_5, Co_2O_3, Co_3O_4 and unreacted precursor were observed, indicating the preparation of pure single-phase $LaCoO_3$ by this method.

The average particle size was estimated from the X-ray line broadening of the diffraction peaks using the Scherrer formula, $D = 0.89\lambda/(h_{1/2}\cos\theta)$, where D is the particle size in nm, λ is the wavelength of the X-ray radiation (0.15418 nm), θ is the Bragg angle and $h_{1/2}$ is the full width at half maximum (FWHM) intensity [46]. Based on a FWHM of the (0 1 2) peak positioned at $2\theta = 23.5^\circ$, we estimate the average particle size to be ~16 nm.

The FT-IR spectra of the precursor and its decomposition product are shown in Fig. 5. In the FT-IR spectrum of precursor (Fig. 5a), the υ(C≡N) stretching band at about 2160 cm^{-1} and $\delta(H_2O)$ band at about 1620 cm^{-1} were observed [47]. The υ(Co–CN) was detected in 450 cm^{-1}. Also, the broad band in the range of 3650–3150 cm^{-1} attributed to υ(OH) of the lattice water molecules. As can be seen in Fig. 5b, all of these bands were disappeared after microwave-assisted decomposition of precursor. In the FT-IR spectrum of the product (Fig. 5b), two strong bands around 620 and 410 cm^{-1} are quite characteristic. These bands correspond to Co–O stretching vibration and O–Co–O bending vibration of CoO_6 octahedra in perovskite $LaCoO_3$, respectively [47,48]. This finding proves the formation of the perovskite $LaCoO_3$ and is in accordance with XRD data.

Fig. 6 shows Raman spectrum of the obtained $LaCoO_3$ nanoparticles in the range of 100–700 cm^{-1}. There are three characteristic peaks at around 135, 415 and 640 cm^{-1} in the Raman spectrum of product, which are very similar to those of $LaCoO_3$ reported in the literature [30,33]. On the other hand, the widening of these lines suggests that the size of particles is very small [49].

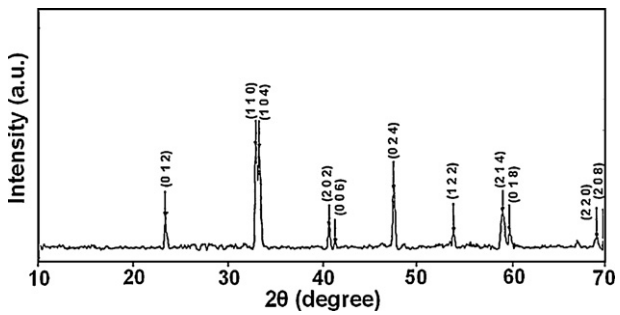

Fig. 4. XRD pattern of the $LaCoO_3$ nanoparticles.

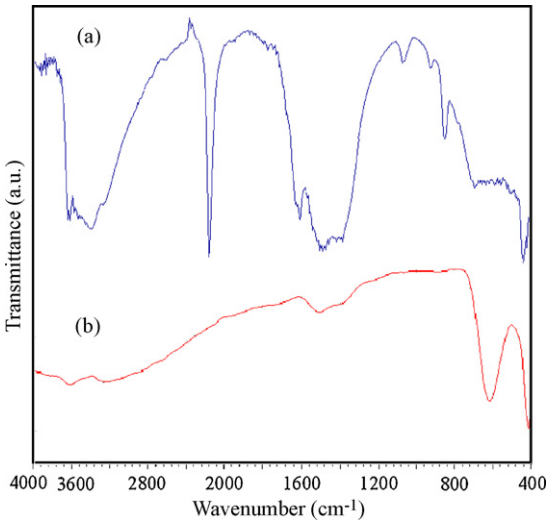

Fig. 5. FT-IR spectra of (a) $La[Co(CN)_6]\cdot 5H_2O$ precursor and (b) $LaCoO_3$ nanoparticles.

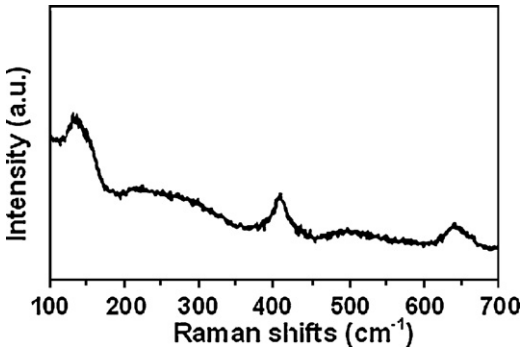

Fig. 6. Raman spectrum of the $LaCoO_3$ nanoparticles.

The obtained $LaCoO_3$ was also examined by XPS for further evaluation of its purity. Fig. 7 shows the XPS spectra of the La 3d and Co 2p core levels. The binding energies of the La $3d_{5/2}$ and Co $2p_{3/2}$ are observed at around 835 and 780 eV, respectively, which are consistent with the literature values of La^{3+} and Co^{3+} [50]. From the peak areas of the La 3d and Co 2p cores, the molar ratio of La to Co was estimated to be 1:1 using the sensitivity factors [50]. So, the composition and valance analysis results of product by XPS also confirm its stoichiometric composition of $LaCoO_3$. The La $3d_{5/2}$ peak

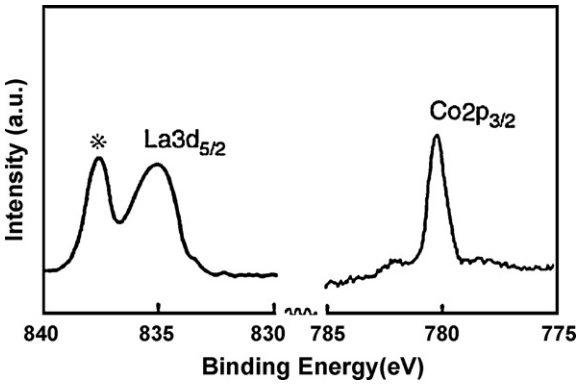

Fig. 7. XPS spectra of the La $3d_{5/2}$ and Co $2p_{3/2}$ levels of the $LaCoO_3$ nanoparticles.

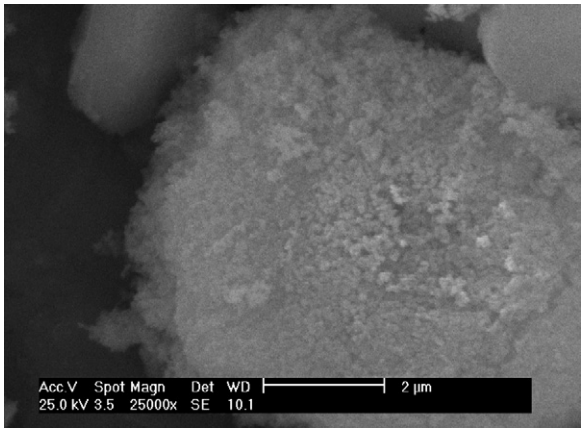

Fig. 8. SEM image of the obtained $LaCoO_3$ powder.

is associated with a strong shoulder at 838.5 eV that is separated from the main peak by ≈3.5 eV. This peak was observed in XPS of other $LaMO_3$ (M = Ti, Cr, Mn, Fe, and Co) and can be interpreted in terms of the excitation of an electron from the anion valence band into the lanthanum 4f band ($O_{2p} \rightarrow La_{4f}$) [51,52].

Fig. 8 shows the SEM image of the obtained $LaCoO_3$ powder. As can be seen, the product consists of extremely fine particles which loosely aggregated. Because of the extremely small dimensions and high surface energy of the obtained $LaCoO_3$ particles, it is easy for them to aggregate as seen in Fig. 8.

TEM image of the obtained perovskite-phase $LaCoO_3$ powder is shown in Fig. 9. TEM sample was prepared with the dispersion of powder in ethanol by ultrasonic vibration. As evident from image, the powder comprises uniform nanoparticles in the range of 10–30 nm. This is consistent with the average size obtained from the peak broadening in X-ray diffraction studied. Such consistence implies that the $LaCoO_3$ nanoparticles are single-phase.

The specific surface area of $LaCoO_3$ nanopowder measured by the BET method to be 27 $m^2\ g^{-1}$ which is the reported greatest value for the pure phase powder of $LaCoO_3$ up to now [31,33]. The particle size was calculated from the data of specific surface area, by the equation $D_{BET} = 6/(\rho S)$, where D_{BET} is the average diameter of a spherical particle, S is the BET specific surface and ρ is the theoretical density of $LaCoO_3$. The average particle size based on this equation is about 17.5 nm which is consistent with XRD and TEM results.

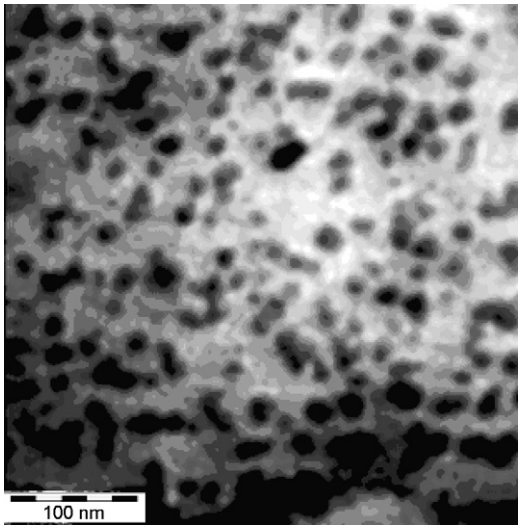

Fig. 9. TEM image of the obtained $LaCoO_3$ powder.

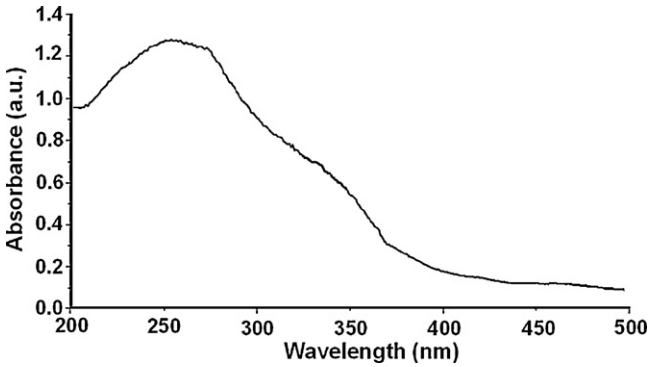

Fig. 10. UV–vis spectrum of the $LaCoO_3$ nanoparticles (*satellite band).

The optical properties of the $LaCoO_3$ nanoparticles was investigated by UV–vis spectroscopy. Fig. 10 shows the UV–vis absorption spectrum of $LaCoO_3$ nanoparticles dispersed in water with a strong absorption at about 265 nm. The strong absorption can mainly be attributed to the band gap electronic transition from the valence band to conduction band ($O^{2-}{}_{2p} \rightarrow Co^{3+}{}_{3d}$). It is clear that sample can absorb the light up to visible region. The spectrum allows us to estimate the optical band gap (E_g) which to be 3.02 eV corresponding to absorption edge close to 410 nm. This indicates that the $LaCoO_3$ nanoparticles prepared by this method could be a kind of photocatalytic material.

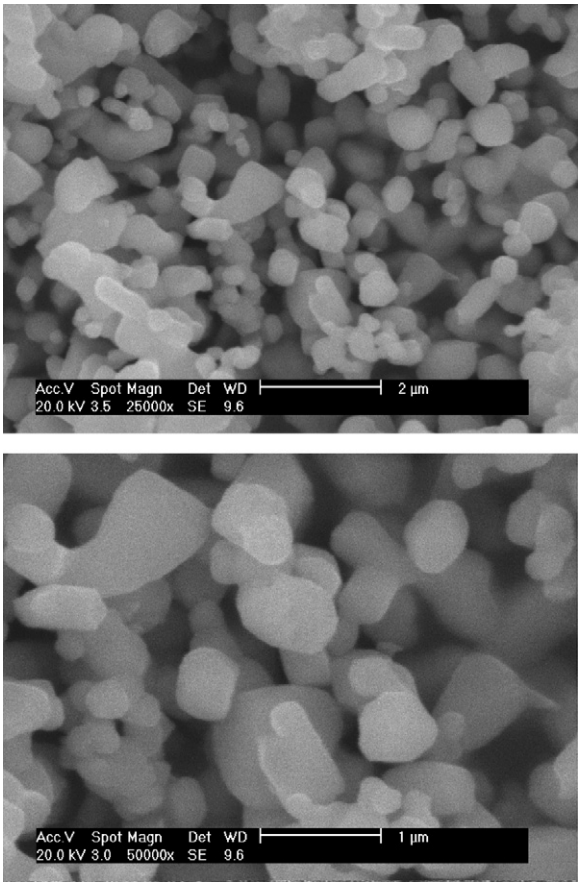

Fig. 11. SEM images (in two different magnifications) of the $LaCoO_3$ powder prepared by thermal decomposition of $La[Co(CN)_6]{\cdot}5H_2O$ in an electric furnace.

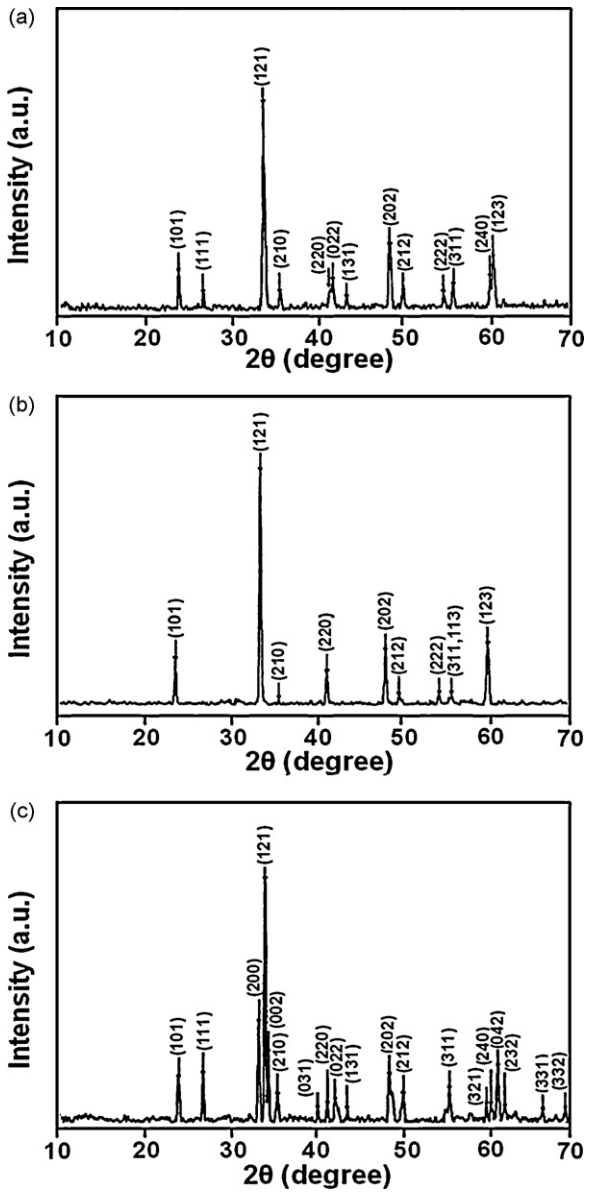

Fig. 12. XRD patterns of microwave-assisted synthesis of (a) $SmCoO_3$, (b) $NdCoO_3$ and (c) $GdCoO_3$ nanoparticles.

In order to make a comparison, the $LaCoO_3$ powder was also prepared by thermal decomposition of $La[Co(CN)_6]\cdot 5H_2O$ in an electric furnace. The XRD and FT-IR results (not shown here) confirmed that the pure phase $LaCoO_3$ was formed at high temperature of 1000 °C after 2 h. For an instance, SEM images of the obtained $LaCoO_3$ by this method are shown in Fig. 11. It is evident that the particle size is in range of 0.2–1 μm.

In Table 1, the preparation time, particle size and specific surface area of $LaCoO_3$ prepared from the decomposition of $La[Co(CN)_6]\cdot 5H_2O$ in microwave oven (the present work) and electric furnace were compared.

From Table 1, it is evident that the use of microwave heating dramatically accelerated reaction rate. Clearly, the reaction time has been reduced by almost 12 times in comparison with the conventional heating (10 min versus 120 min, Table 1). In addition, the microwave synthesis of $LaCoO_3$ gives smaller particles with higher specific surface area. The decreased crystal size might be related with the increased nucleation rate. The nucleation rate should be high because of high heating rate under microwave irradiation.

Table 1
Comparison between the properties of $LaCoO_3$ prepared from solid-state decomposition of $La[Co(CN)_6]\cdot 5H_2O$ by microwave heating and conventional heating.

Properties	Decomposition method	
	Microwave heating[a]	Conventional heating[b]
Reaction conditions	900 W, 10 min, in air	1000 °C, 120 min, in air
Particle size (nm)[c]	10–30	200–1000
Average particle size (nm)[d]	16	500
Specific surface area ($m^2\ g^{-1}$)[e]	27	6.5

[a] In a domestic microwave oven.
[b] In an electric furnace.
[c] Estimated by TEM/SEM images.
[d] Calculated by the Scherrer formula.
[e] Calculated from N_2 adsorption measurement by BET method.

The difference in morphology of products from two reaction methods also shows that the reaction mechanism differs from each other.

3.2. Preparation of $SmCoO_3$, $NdCoO_3$ and $GdCoO_3$ nanoparticles

The synthesis of other lanthanide cobaltites, $LnCoO_3$ (Ln = Sm, Nd, Gd) have also been carried out through the present method. The nanoparticles of these oxides were prepared in a similar manner with $LaCoO_3$ by the microwave-assisted decomposition of their corresponding bimetallic complexes, $Ln[Co(CN)_6]$ (Ln = Sm, Nd, Gd), within 10 min. Fig. 12 shows the XRD patterns of the obtained products. All cases give us the patterns of $SmCoO_3$ (JCPDS card no. 8-0149), $NdCoO_3$ (JCPDS card no. 25-2064) and $GdCoO_3$ (JCPDS card no. 25-1057) as pure and single-phase. The results indicate that the present method is useful to prepare nano-sized and homogeneous perivskite-type ABO_3 materials.

4. Conclusion

$LaCoO_3$ can be simply synthesized by rapid decomposition of the $La[Co(CN)_6]\cdot 5H_2O$ under microwave irradiation with the assistance of CuO as the secondary heater. The obtained $LaCoO_3$ nanoparticles have narrow size distribution (10–30 nm) with high specific surface area (27 $m^2\ g^{-1}$). The smaller particles of the $LaCoO_3$ with high purity and short reaction time are other significant advantages of this method compared with most reported methods. This method has been used for synthesizing other $LnCoO_3$ such as $SmCoO_3$, $NdCoO_3$ and $GdCoO_3$ and we foresee that the $LaCoO_3$ nanoparticles are more attractive in electrical and catalytic applications. This method is promising for preparation of other mixed oxide and related compounds.

Acknowledgement

The authors are grateful for the financial support of the Lorestan University Research council.

References

[1] N.Q. Minh, J. Am. Ceram. Soc. 76 (1993) 563–588.
[2] M.B. Phillipps, N.M. Sammes, O. Yamamoto, J. Mater. Sci. 31 (1996) 1689–1692.
[3] S.P. Jiang, L. Liu, P.O.B. Khuong, W.B. Ping, H. Li, H. Pu, J. Power Sources 176 (2008) 82–89.
[4] X.F. Ding, Y.J. Liu, L. Gao, L.C. Guo, J. Alloys Compd. 425 (2006) 318–322.
[5] S. Srinvasan, B.B. Dave, K.A. Murugesamoorthi, A. Partasarathy, A.J. Appleby, in: L.J.M.J. Blomen, M.N. Mugerwa (Eds.), Solid Oxide Fuel Cells in Fuel Cell Systems, New York, Plenum, 1993, pp. 58–63.
[6] M. Shiono, K. Kobayashi, T.L. Nguyen, K. Hosoda, T. Kato, K. Ota, Solid State Ionics 170 (2004) 1–7.
[7] M.A. Pena, J.L.G. Fierro, Chem. Rev. 101 (2001) 1981–2017.

[8] D.T. Anh, W. Olthuis, P. Bergveld, Sens. Actuator B: Chem. 103 (2004) 165–168.
[9] X. Liu, B. Cheng, J.F. Hu, H.W. Qin, M.H. Jiang, Sens. Actuator B: Chem. 129 (2008) 53–58.
[10] L.B. Kong, Y.S. Shen, Sens. Actuator B: Chem. 30 (1996) 217–221.
[11] Y. Teraoka, H.M. Zhang, S. Furukawa, N. Yamazoe, Chem. Lett. (1985) 1743–1746.
[12] A. Weidenkaff, R. Robert, M. Aguirre, L. Bocher, T. Lippert, S. Canulescu, Renew. Energy 33 (2008) 342–347.
[13] K.S. Song, H.X. Cui, S.D. Kim, S.K. Kang, Catal. Today 47 (1999) 155–160.
[14] M. O'Connell, A.K. Norman, C.F. Huttermann, M.A. Morris, Catal. Today 47 (1999) 123–132.
[15] R. Spinicci, M. Faticanti, P. Marini, S. De Rossi, P. Porta, J. Mol. Catal. A: Chem. 197 (2003) 147–155.
[16] R. Doshi, C.B. Alcock, J.J. Carberry, Catal. Lett. 18 (1993) 337–343.
[17] R.J.H. Voorhoeve, J.P. Remeika, L.E. Trimble, A.S. Cooper, F.J. Disalvo, P.K. Gallagher, J. Solid State Chem. 14 (1975) 395–406.
[18] F. Gaillard, X.G. Li, M. Uray, P. Vernoux, Catal. Lett. 96 (2004) 177–183.
[19] V. Szabo, M. Bassir, A. Van Neste, S. Kaliaguine, Appl. Catal. B: Environ. 37 (2002) 175–180.
[20] F.M. Figueiredo, J.R. Frade, F.M.B. Marques, Solid State Ionics 118 (1999) 81–87.
[21] S.C. Parida, Z. Singh, S. Dash, R. Prasad, V. Venugopal, J. Alloys Compd. 285 (1999) 7–11.
[22] T. Yao, A. Ariyoshi, T. Inui, J. Am. Ceram. Soc. 80 (1997) 2441–2444.
[23] A.D. Jadhav, A.B. Gaikwad, V. Samuel, V. Ravi, Mater. Lett. 61 (2007) 2030–2032.
[24] S. Nakayama, M. Okazakib, Y.L. Aunga, M. Sakamotoc, Solid State Ionics 158 (2003) 133–139.
[25] Y. Zhu, R. Tan, T. Yi, S. Ji, X. Ye, L. Cao, J. Mater. Sci. 35 (2000) 5415–5420.
[26] D. Berger, V. Fruth, I. Jitaru, J. Schoonman, Mater. Lett. 58 (2004) 2418–2422.
[27] Y. Sadaoka, E. Traversa, M. Sakamoto, J. Alloys Compd. 240 (1996) 51–59.
[28] L. Amelao, G. Bandoli, D. Barreca, M. Bettinelli, G. Bottaro, A. Caneschi, Surf. Interface Anal. 34 (2002) 112–115.
[29] G. Sinquin, C. Petit, J.P. Hindermann, A. Kiennemann, Catal. Today 70 (2001) 183–196.
[30] M. Popa, J. Frantti, M. Kakihana, Solid State Ionics 154–155 (2002) 135–141.
[31] M. Popa, M. Kakihana, Solid State Ionics 151 (2002) 251–257.
[32] M. Popa, L. Van Hong, M. Kakihana, Physica B 327 (2003) 233–236.
[33] M. Popa, J.M. Calderon-Morena, J. Eur. Ceram. Soc. 29 (2009) 2281–2287.
[34] D.M.P. Mingos, D.R. Baghurt, Chem. Soc. Rev. 20 (1991) 1–47, and references cited therein.
[35] K.J. Rao, B. Vaidhyanathan, M. Ganguli, P.A. Ramakrishnan, Chem. Mater. 11 (1999) 882–895.
[36] M. Panneerselvam, K.J. Rao, J. Mater. Chem. 13 (2003) 596–601.
[37] M. Nakayama, K. Watanabe, H. Ikuta, Y. Uchiharu, M. Wakihara, Solid State Ionics 164 (2004) 35–42.
[38] I. Ganesh, B. Srinivas, R. Johnson, B.P. Saha, Y.R. Mahajan, J. Eur. Ceram. Soc. 24 (2004) 201–207.
[39] P. Elomalai, H.N. Vasan, N. Munichandraiah, J. Power Sources 125 (2004) 77–84.
[40] H.Y. Xu, H. Wang, Y.Q. Meng, H. Yan, Solid State Commun. 130 (2004) 465–468.
[41] J. Guo, C. Dong, L. Yang, G. Fu, J. Solid State Chem. 178 (2005) 58–63.
[42] C. Mastrovito, J.W. Lekse, J.A. Aitken, J. Solid State Chem. 180 (2007) 3262–3264.
[43] N. Takahashi, Mater. Lett. 62 (2008) 1652–1654.
[44] X. Song, L. Gao, J. Am. Ceram. Soc. 91 (2008) 3465–3468.
[45] S. Farhadi, M. Momeni, M. Taherimehr, J. Alloys Compd. 471 (2009) L5–L8.
[46] H.P. Klug, L.E. Alexander, X-ray Diffraction Procedures, second ed., Wiley, New York, 1964.
[47] K. Nakamoto, Infrared and Raman Spectra of Inorganic and Coordination Compounds, Part B: Applications in Coordination, Organometallic and Bioinorganic Chemistry, sixth ed., Wiley, New York, 2009, pp. 110–120.
[48] G.V.S. Rao, C.N.R. Rao, J.R. Ferraro, Appl. Spectrosc. 24 (1970) 436–445.
[49] M.J. Pelletier, Analytical Applications of Raman Spectroscopy, Blackwell Science, Oxford, 1999.
[50] C.D. Wagner, Handbook of X-ray Photoelectron Spectroscopy, Perkin-Elmer Corporation, Minnesota, 1979.
[51] D.J. Lam, B.W. Veal, D.E. Ellis, Phys. Rev. B 22 (1972) 5730–5742.
[52] M.M. Natile, E. Ugel, C. Maccato, A. Glisenti, Appl. Catal. B: Environ. 72 (2007) 351–362.